Adsorbate-induced segregation: First-principles study for C/$Pt_{25}Rh_{75}$(100)

Tobias C. Kerscher,[1,2,*] Wolfgang Landgraf,[3] Raimund Podloucky,[2] and Stefan Müller[1]
[1]*Hamburg University of Technology, Institute of Advanced Ceramics, Denickestraße 15, 21073 Hamburg, Germany*
[2]*University of Vienna, Department of Physical Chemistry, Sensengasse 8/7, 1090 Vienna, Austria*
[3]*Lehrstuhl für Festkörperphysik, Staudtstraße 7, 91058 Erlangen, Germany*
(Received 25 September 2012; revised manuscript received 7 November 2012; published 19 November 2012)

We develop a cluster-expansion (CE) formalism for the first-principles study of substrate-adsorbate interaction in order to study adsorbate-induced segregation. The simulation lattice, the configuration space, and the basis functions of the CE are bisected into separate but interacting subsystems. The method is applied to the C-contaminated $Pt_{25}Rh_{75}$(100) surface. For such catalytic surfaces, it is essential to understand the change in the segregation profile of the substrate due to the presence of adsorbates. In accordance with experiments, we find that even a small amount of C impurities leads to a considerable decrease in the Pt segregation to the topmost substrate layer. We discuss the coupling of the substrate with the adsorbate layers in the CE Hamiltonian, the $T = 0$ K stability diagram of C/$Pt_{25}Rh_{75}$(100), and our prediction of the temperature-dependent segregation profile for different C contaminations.

DOI: 10.1103/PhysRevB.86.195420 PACS number(s): 68.43.Fg, 71.15.Mb, 71.15.Nc

I. INTRODUCTION

The binary alloy of platinum and rhodium is especially known for the catalytic properties of its surfaces.[1–4] Not surprisingly, various publications have already attended to the same system; for example, Refs. 3–8 discuss the relevancy of Pt-Rh in three-way catalysts, and some empirical models about the catalytic process are developed in Refs. 9–11. The present work takes two steps back: first, because the whole alloy Pt-Rh will be brought down to its atomic constituents, and second, because not the dynamics of the catalytic process itself will be under investigation but, more fundamentally, the equilibrium properties of Pt-Rh. This approach joins with other atomistic works on Pt-Rh surfaces, experimental papers such as Refs. 12 and 13, as well as numerous theoretical surveys such as Refs. 14–18. However, all those theoretical publications do not address the equilibrium properties of the surface contaminated by an adsorbate. But an adsorbate on top of a substrate such as Pt-Rh is the whole basis behind catalysis, and indeed, an adsorbate can make a decisive difference on the composition of a binary catalytic surface.

The clean (noncontaminated) surfaces of Pt-Rh are well known to show the segregation of Pt to the topmost surface layer. Experimental data[12,13,19–24] as well as theoretical studies[16–18,25–27] document the Pt enrichment in the first layer, and Ref. 28 even reports the platinum's preference to stay on top in Pt-Rh nanoparticles. The multitude of experimental and theoretical investigations mirror the importance of the alloy's surface for catalytic reactions, and they reflect different approaches to the field of segregation: There are experimental data obtained via low-energy electron diffraction (LEED) and low-energy ion scattering (LEIS),[12] via Auger electron spectroscopy (AES),[12,21] and via chemically resolved scanning tunneling microscopy (STM) images.[23] Likewise, the theoretical playground comprises tight-binding approaches and the coherent potential approximation (CPA),[25] a first-nearest-neighbor embedded-atom potential (EAM),[27] and *ab initio* approaches in combination with a cluster expansion.[16,18]

This segregation profile of the clean alloy substrate can change by the presence of an adsorbate such as oxygen, carbon, or carbon compounds; an effect called *adsorbate-induced segregation*. For carbon on top of a $Pt_{25}Rh_{75}$(100) surface, adsorbate-induced segregation was experimentally observed and gauged by Platzgummer *et al.*,[12] and for oxygen by Baraldi *et al.*[29] The presence of carbon influences the segregation profile, but oxygen even results in an oxygen-induced (3×1) reconstruction of the surface.[30] In the following, we restrict ourselves to the adsorption of carbon on the surface.

Our atomistic approach is based on first-principles density-functional theory (DFT) calculations which are used as input for a cluster-expansion (CE) Hamiltonian.[31–36] As already demonstrated earlier for the $Pt_{25}Rh_{75}$(100) surface,[18] the CE is a powerful tool to predict the segregation profile of metal alloys. In the present paper, we extend the formalism further (as in Refs. 34 and 35) for the modeling of the layer-by-layer segregation behavior under the influence of an adsorbate; for the technical details, see Sec. II below.

In order to appropriately model the (100) surface of $Pt_{25}Rh_{75}$ by a slab in the DFT calculation, the underlying bulk structure must be known because a thorough understanding of the bulk ordering phenomena is crucial for meaningful models of the various Pt-Rh surfaces. Until recently, the literature about the ordering properties within the bulk region and its corresponding phases was both sparse and contradictory.[14,37–40] Our recent *ab initio* study[41] predicts the $D0_{22}$ bulk structure as a ground-state for 25% Pt. This agrees with the prior theoretical study of Pohl *et al.*[40] Even so, for our surface studies the $D0_{22}$-like ordering in the bulk can be replaced by the $L1_2$-type bulk structure which tremendously cuts down the computational cost. The rationale for this approximation will be given in Sec. II below.

As knowledge about bulk ordering must precede any surface study, so must fundamental knowledge about the equilibrium properties of surfaces under the influence of adsorbates precede investigations of the single steps of a catalytic reaction. The work presented here builds on our prior *ab initio* investigations of both bulk and surface properties of Pt-Rh.[18,41] In the following, we will set up a CE Hamiltonian for the adsorbate-substrate system (Sec. II) and discuss the CE predictions as well as results of thermodynamic Monte Carlo

 ©2012 American Physical Society

(MC) simulations for the equilibrium segregation behavior of $Pt_{25}Rh_{75}(100)$ contaminated by C (Sec. III).

II. A COUPLED CE HAMILTONIAN

A. General aspects of the CE

The CE is about mastery over the configuration space $\Sigma_L^N(k)$, which is the set of all different atomic configurations with k components on a given lattice L with N sites; k is called the rank of the CE. For subjugating the configuration space, a standard CE Hamiltonian

$$E(\sigma) = \sum_{C \in \boldsymbol{C}} J_C \Pi_C(\sigma), \tag{1}$$

can be employed, where the energy $E(\sigma)$ of an arbitrary atomic structure $\sigma \in \Sigma_L^N(k)$ is expressed in the form of a generalized Ising model.[31] For the setup of a CE Hamiltonian like Eq. (1), we use our UNCLE code.[36] In Eq. (1), a cluster C represents the interaction between v lattice sites ($v = 0,1,2,\ldots$). To this end, we define a cluster C as a composite object comprising both a geometrical figure and algebraic information about the basis functions of the expansion. The geometric figure connects the v interacting lattice sites, which are occupied by k different mathematical spins that stand for different atomic species; the algebraic information is necessary for the evaluation of the correlations $\Pi_C(\sigma)$, which form the basis functions of the expansion Eq. (1) and incorporate the structure dependence of $E(\sigma)$ by a product of functions (exactly defined by the particular algebraic information within C) which depend on the occupational spins of the cluster C on the lattice (not shown).[31,36,42] The free parameters $\{J_C\}$ (the so-called effective cluster interactions) account for the interaction strength of a certain cluster C. The numerical value of the $\{J_C\}$ is determined by least-squares fitting in such a way that the CE sum Eq. (1) reproduces the energetics of a set of relaxed DFT input structures. Furthermore, a genetic algorithm[43] in UNCLE[36] tries to find a cluster set $\boldsymbol{C}$, which describes the energetics in a way as optimal as possible; the more clusters that can be defined on the lattice, the harder it is to find such a good set. If the CE predicts energetically favorable structures that were not included in the DFT input set, then DFT calculations are performed for those structures, the structures and their DFT energetics are added to the input set, and the CE is set up anew until the CE is self-consistent.[44] (For a more thorough view on some practical aspects of CEs in general, see Refs. 36 and 45.)

The more complex the configuration space, the harder it is to scan it in its entirety and to find its most important configurations via Eq. (1). For the study of adsorbate-induced segregation, there are three main reasons for the increase in complexity for the CE; the first one directly influences the configuration space, while the second and the third ones simply increase the number of clusters C which have to be used in Eq. (1). The first reason for the rising complexity of the CE is the large symmetry-breaking surface slabs, which tremendously increase the cardinality of the configuration space with every additional parent unit cell taken into account. Second, the lattices thus defined result in numerous different, symmetrically inequivalent clusters C in Eq. (1), which also increase the amount of DFT calculations for the determination of $\{J_C\}$. And lastly, the presence of an adsorbate increases the rank of the CE not merely by 1, but generally by 2: not only must the configuration space account for the presence of the adsorbate but it must also include the absence of the adsorbate on all other adsorption sites. As a higher rank changes the algebraic information of the clusters and thus the construction of the correlations $\Pi_C(\sigma)$,[31,36,42,46] it effectively results in more symmetrically inequivalent clusters C on a given lattice, and a CE also needs more clusters C to converge Eq. (1) towards self-consistency.

In order to proceed, we first need to discuss the lattice, on which the Pt-Rh substrate and the C adsorbate are placed (Sec. II B), and then we need to find an efficient method for the description of adsorbate-induced segregation (Sec. II C). Finally, the effective interactions $\{J_C\}$ are determined by DFT calculations, whose parameters are summarized in Sec. II E.

B. Model lattice

The model lattice L has to incorporate the $Pt_{25}Rh_{75}(100)$ substrate, the C adsorbate, and the "C-vacancies". So in total, four different atomic "species" are distributed over the lattice and *a priori* $k = 4$, which will fortunately change in due course. Our choice for L was a symmetric surface slab with three bulk-like layers and five surrounding surface-like layers. The former fixed the lateral lattice constant, and the latter provided room for both the substrate (four layers) and the adsorbate (one layer).

The four (100) substrate layers can accommodate arbitrary Pt and Rh occupations in fcc like positions; both our previous theoretical studies for clean surfaces[18] and experimental data[12] have shown that four layers suffice for the model. The substrate layers build around three bulk-like fcc layers with fixed $Pt_{25}Rh_{75}$ occupation, arranged in an $L1_2$ structure—in opposition to the genuine bulk ground-state structure $D0_{22}$.[40,41] The reason for preferring $L1_2$ over $D0_{22}$ is the reduced cost of DFT calculations for a surface slab by using the smallest possible slab unit cell. Both structure types exhibit the same Pt chains, and careful energetic considerations by DFT showed that the segregation energies of Pt from the second to the first (i.e., topmost) surface layer—and hence the tendency of Pt to segregate—differ only by 1%, namely, 4 meV per 1×1 lateral surface unit cell. This is a result of the configurational similarity of the two structures and specifically of the very similar *ab initio* lattice constant of both structures. The fact that the segregation energies coincide for the bulk structures $D0_{22}$ and $L1_2$, as well as the success of Ref. 18 to predict the experimentally observed segregation behavior, ratify the use of $L1_2$ as the pseudo-bulk structure in the slab. This setup leaves us with 11 slab layers for the $Pt_{25}Rh_{75}(100)$ substrate and a 2×1 lateral unit cell due to the $L1_2$ bulk structure. The amount of Pt in the four substrate layers will be denoted by x.

On top of the substrate layers, one additional layer accommodates the C contaminants. In our model, the C atoms can be placed on different fcc sites: the lateral 2×1 substrate lattice allows for two top, four bridge, and two hollow adsorption sites. So, the maximum coverage is $\Theta = 4$ ML (monolayers).

We note that the surface slab thus constructed forms a parent lattice L that can be bisected into two separate systems by

$$L = L_S \otimes L_A, \tag{2}$$

namely, a sublattice L_S of the substrate with Pt and Rh atoms and a sublattice L_A of the adsorbate layer with C atoms and "C vacancies". Also noteworthy with respect to the CE is the change in lateral lattice site symmetry induced by the $L1_2$ bulk structure.

C. Bi-binary CE for the substrate-adsorbate system

For surfaces—and, hence, also for general substrate-adsorbate problems—a fully-converged CE Hamiltonian of the form Eq. (1) is in need of too many clusters C, too many effective interactions J_C, and too many DFT calculations. When Drautz *et al.*[47] first constructed a surface CE for the $Ni_{90}Al_{10}(110)$ surface, they exploited the fact that energies are additive and used a reference energy as an estimate for the true energy of a surface structure. This procedure reduced the number of DFT calculations necessary to determine the effective interactions for a fully converged CE and made the surface CE possible at all. We can as well apply the very same procedure here: Energy references relieve the CE of putting all energetics into a *single* CE; instead, the energy is split into two or more parts, making the CE more efficient. For all that, we will first examine a different approach in the present section: it will not break apart the energetics, but will rather split the configuration space. This relieves the CE of scanning a *single* impenetrable configuration space; instead, the configuration space itself is cut into several subspaces.

A system is well suited for such a split-up of the total configuration space if it already separates into two or more subsystems from a physical point of view. The subsystems must be distinct and separate from each other, they are forbidden to share a common atomic occupation, and so the atoms in one of the subsystems must not be able to be present in another subsystem. This physical situation—namely, that the subsystems do not mix—is present in our case of an adsorbate on top of a substrate, which can be modeled according to Sec. II B by two different sublattices L_A and L_S of the parent lattice $L = L_S \otimes L_A$.

Given those prerequisites and taking the separation of the systems for granted, not only the lattice L but also the configuration space can be bisected into a combination of the substrate's configuration space and the adsorbate's configuration space:

$$\Sigma_L^N(4) = \Sigma_{L_S \otimes L_A}^N(4) = \Sigma_{L_S}^{N_S}(2) \otimes \Sigma_{L_A}^{N_A}(2). \tag{3}$$

Not only the configuration space and hence the comprehensive scan by the cluster expansion profit from the separation into several subsystems; but also the very construction of the cluster expansion gains from it since the coupling Eq. (3) turns the total system of rank $k = 4$ into two subsystems with lower rank, namely, $k = 2$: the substrate system accommodates Pt and Rh, the adsorbate system C, and C vacancies. As an immediate consequence of the reduced rank, the number of symmetrically inequivalent clusters C for the CE decreases drastically, see Sec. II A.

Therefore, the lattice coupling of Eq. (2) eases the first and the third burdens that increase the complexity of a CE as described in the second paragraph of Sec. II A: By Eq. (3), the configuration space is reduced, and also the additional clusters C that would arise in a quaternary CE (rank $k = 4$) were eliminated by breaking the configuration space into two binary ("bi-binary") spaces. In combination, these two advantages make the coupling between two separate lattices Eq. (2) an ideal tool for studying, for example, the binary $Pt_{25}Rh_{75}(100)$ surface with a binary adsorbate layer. While here we will use four substrate layers coupled with one adsorbate layer, we note that UNCLE[36] is built in such a way as to allow for an arbitrary number of layers and lattice couplings. The generalizations of Eqs. (2) and (3) required for this are straightforward.

This work is not the first to propose a coupling of physically different subsystems. We will compare our work with other publications in Sec. II F.

Being $\tilde{\sigma}$ and $\tilde{\alpha}$ the surface structures on the multi-lattice L_S and the adsorbate structures on the multi-lattice L_A, respectively, the combined "substrate-adsorbate" structures are given by

$$\sigma = (\tilde{\sigma}, \tilde{\alpha}) \in \mathbf{\Sigma}_{L_S}^{N_S}(2) \otimes \mathbf{\Sigma}_{L_A}^{N_A}(2). \tag{4}$$

In a full CE for these substrate-adsorbate structures the form of the configuration space Eq. (3) must be reflected in the form of the basis functions of the CE, namely, the correlations $\Pi_C(\sigma)$. With the configuration space as a bi-binary product space, the correlation functions also follow the product representation, which is then passed on to the definitions of clusters:

$$E(\tilde{\sigma}, \tilde{\alpha}) = \sum_{C_S, C_A} J_{C_S C_A} (\Pi_{C_S}(\tilde{\sigma}) \otimes \Pi_{C_A}(\tilde{\alpha})) \tag{5}$$

$$=: \sum_{C \in \boldsymbol{C}} J_C \Pi_C(\tilde{\sigma}, \tilde{\alpha}), \tag{6}$$

with the substrate clusters $C_S \in \boldsymbol{C}_S$ and the adsorbate clusters $C_A \in \boldsymbol{C}_A$—i.e., all C_S only connect sites of the surface substrate layers, and all C_A only connect sites of the adsorbate layer.

What are the implications of the new basis functions $\Pi_{C_S}(\tilde{\sigma}) \otimes \Pi_{C_A}(\tilde{\alpha})$ of Eq. (5)? Effectively, they result in a new total cluster set, $\boldsymbol{C} = \boldsymbol{C}_S \otimes \boldsymbol{C}_A$ in Eq. (6), by the introduction of which the original form of the CE could be regained. This new cluster set comprises clusters that couple the two systems with each other. Specifically, it contains the clusters within S, the clusters within A, as well as those clusters that truly connect the two systems with each other:

$$\boldsymbol{C} = \boldsymbol{C}_S \otimes \boldsymbol{C}_A = \boldsymbol{C}_S \cup \boldsymbol{C}_A \cup \boldsymbol{C}_{S-A}. \tag{7}$$

Figure 1 demonstrates how the cluster set $\boldsymbol{C} = \boldsymbol{C}_S \otimes \boldsymbol{C}_A$ evolves from the clusters in S and the clusters in A. This piecewise construction of $\boldsymbol{C}$ reproduces the structure of the configuration space itself.

D. Construction of a CE for C/$Pt_{25}Rh_{75}$(100)

Having found a formal way to define a CE Hamiltonian for the coupled substrate-adsorbate system in the previous section, we will now discuss the actual construction of a CE for C/$Pt_{25}Rh_{75}$(100). Our construction will use reference energies from a previously conducted surface CE and also an averaging procedure of different CE Hamiltonians.

The energetics of a clean $Pt_{25}Rh_{75}(100)$ substrate provide the canonical starting point for the C-contaminated substrate. Therefore, a surface CE Hamiltonian like the one of our

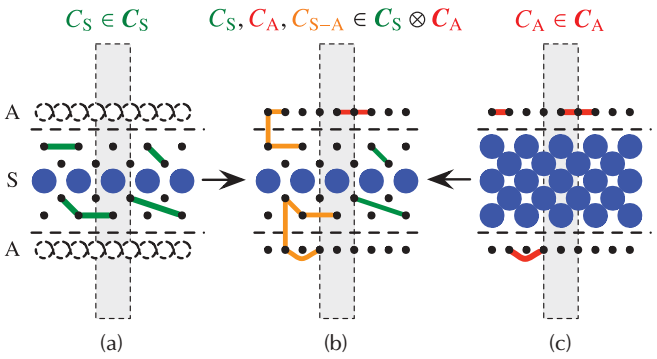

FIG. 1. (Color online) Schematic side view of a substrate-adsorbate slab with "blue" bulk occupation. Lattice sites with arbitrary substrate occupation in S or adsorbate occupation in A are denoted by black dots. Two limit cases are shown in (a) and (c) where effectively no coupling takes place because one of the systems has fixed occupations, while (b) demonstrates a true coupling situation, where all the clusters used are within $\boldsymbol{C}_S \otimes \boldsymbol{C}_A$.

publication Ref. 18 provides a first estimate $E^{\text{surf}}(\tilde{\sigma})$ for the energy $E(\sigma)$ of a structure $\sigma = (\tilde{\sigma},\tilde{\alpha})$. With the help of this clean-surface reference, we put up n_a bi-binary cluster-expansion Hamiltonians of the form

$$E_i(\sigma) = E^{\text{surf}}(\tilde{\sigma}) + \sum_{C \in \boldsymbol{C}_i \subset \boldsymbol{C}_S \otimes \boldsymbol{C}_A} J_C \Pi_C(\tilde{\sigma},\tilde{\alpha}) \qquad (8)$$

with $i = 1, \ldots, n_a$.

Apart from the help a reference energy provides, we note again that in particular the bisection of the configuration space Eq. (3) assists the construction of a CE like Eq. (8): The reduced configuration space helps because the cluster expansion must be valid for fewer configurations, and the reduced rank (2 instead of 4) helps because the genetic algorithm in UNCLE can select the best clusters more easily.

In spite of that, the configuration space is still highly complex. The configuration space is already reduced, and yet almost 400 DFT input energies were needed for the stabilization of the CE in the concentration region $0 \leqslant x \leqslant 0.5$ for the platinum content in the four substrate layers and $0 \leqslant \Theta \leqslant 0.5$ for the carbon coverage. The rank of the problem is lowered and far fewer clusters make up the pool of inequivalent clusters, and yet it is extremely difficult to select an appropriate set of clusters. Therefore, we follow the recent approach by Reith *et al.*[48] and apply an averaging procedure. Our final substrate-adsorbate CE for C/$Pt_{25}Rh_{75}$(100) was constructed as an average of $n_a = 328$ separate Hamiltonians of the form of Eq. (8):

$$\bar{E}(\tilde{\sigma},\tilde{\alpha}) = E^{\text{surf}}(\tilde{\sigma}) + \frac{1}{n_a} \sum_{i=1}^{n_a} \sum_{C \in \boldsymbol{C}_i} J_C \Pi_C(\tilde{\sigma},\tilde{\alpha}). \qquad (9)$$

This procedure yielded a total of over 10000 clusters in the sum of Eq. (9) and an rms error of 2.4 meV/(slab site) = 22.8 meV/(1 × 1 surface cell) between CE energies and DFT energies for the input structures.

Given the energy $\bar{E}(\tilde{\sigma},\tilde{\alpha})$, one can also calculate the adsorption energy $E_{\text{ads}}(\tilde{\alpha}|\tilde{\sigma})$, which measures the energy gained or lost by the adsorption of $\tilde{\alpha}$ on top of the substrate structure $\tilde{\sigma}$, and also the energy of formation for the substrate-adsorbate structure,

$$E_f(\tilde{\sigma},\tilde{\alpha}) = E_f(\tilde{\sigma}) + E_{\text{ads}}(\tilde{\alpha}|\tilde{\sigma}), \qquad (10)$$

which combines the formation energy of the clean surface, $E_f(\tilde{\sigma})$, with the adsorption energy $E_{\text{ads}}(\tilde{\alpha}|\tilde{\sigma})$.

E. DFT input for the CE

Our DFT calculations for C/$Pt_{25}Rh_{75}$(100) used the Vienna Ab-initio Simulation Package (VASP)[49–53] together with projector augmented wave (PAW) potentials[53,54] and the GGA-PW91 parametrization[55] for the exchange-correlation energy. The bulk layers of the slab fixed the lateral lattice parameter; all other degrees of freedom were fully relaxed in several steps. The method of Monkhorst and Pack[56] was employed for sampling the reciprocal space, the exact form of which was adjusted to the size and form of the slab superlattice.

F. Comparison with other publications

Our strategy in the previous paragraphs was to dissect a system into different subsystems, Eq. (2), which influences the configuration space, Eqs. (3) and (4), and results in a CE Hamiltonian, Eq. (6), that couples different systems. The principle of this strategy is not totally new, as we have already noted in Sec. II C and as will be discussed in the next paragraphs. However, our work clearly contrasts with prior publications in its generality and application to a complex surface-adsorbate problem.

In 1995, Tepesch *et al.*[34] used a coupled CE approach for bulk model systems with distinct sublattices, which separately house the anions and cations. A followup study, more closely related to our work, was conducted by Han *et al.*,[35] and they indeed applied a coupled CE to a surface-adsorbate system. Yet, we want to point out the differences between the work of Ref. 35 and our work in order to justify our approach.

In Ref. 35, the authors studied surface segregation in O/Pt-Ru(111) on a very simple surface model with only one actual surface substrate layer; the deeper substrate layers were modeled as a reservoir of atoms by a grand-canonical approach with a given chemical potential. Even though the present work makes use of the same principle formalism—namely, the coupled CE—it generalizes this elementary model to an arbitrary number of substrate layers, which enables the profound study of interfacial phenomena such as surface segregation on a much broader basis. At first sight, this generalization might seem unexceptional, but the consequences of our approach are demanding: the different substrate layers result in many symmetrically inequivalent clusters which hamper the convergence of the CE and make an averaging procedure necessary (as laid out in Sec. II D), but the setup of different substrate layers also enables us to study the segregation profile layer-by-layer.

III. RESULTS AND DISCUSSION

The averaged CE Hamiltonian Eq. (9) for the substrate-adsorbate system C/$Pt_{25}Rh_{75}$(100) enabled us to examine the whole configuration space of interest. In the following, we will first discuss the stability of the system at $T = 0$ K and will then

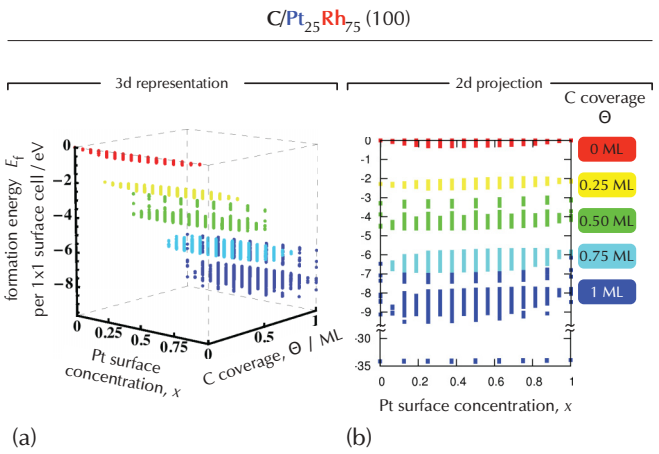

FIG. 2. (Color online) Configurational scan with the averaged CE of Eq. (9) over the configuration spaces discussed in the main text. For C coverages $\Theta \leqslant 0.5$ ML the hollow sites form the most stable adsorbate structures (not shown). It is only for $\Theta = 1$ ML that the C atoms clump together by forming carbon-carbon bonds between top, hollow, and bridge positions. The energy of those bonds is highly overestimated by the cluster expansion, as visible in (b). In total, 612900 substrate-adsorbate structures ($\tilde{\sigma}$,$\tilde{\alpha}$) are shown.

proceed towards the segregation profile at higher temperatures by means of MC simulations.

A. Stability behavior

The energetics of a configurational scan in the concentration region $0 \leqslant x \leqslant 1$ (substrate Pt concentration) and $0 \leqslant \Theta \leqslant 1$ (C coverage) is shown in Fig. 2. The figure nicely shows how the formation energy Eq. (10) decreases in a step-like structure when the carbon coverage is increased. The steps are due to the increase in adsorption energy: When more carbon atoms bind to the surface, the amount of energy released by the adsorption grows, approximately by the rule that two independently adsorbed carbon atoms release roughly two times the adsorption energy of one single carbon atom. The configurational scan of Fig. 2 was only practicable for all possible adsorption sites (four per standard 1×1 lateral unit cell) within a 2×1 slab. For supercells constructed out of two 2×1 unit cells, the algorithm had to restrict adsorption to the hollow sites (one per standard 1×1 lateral unit cell). Owing to the difference in possible adsorption sites in Fig. 2, the energies vary much more for the small supercells (with top, bridge, and hollow adsorption sites) than for the larger supercells (with hollow adsorption sites only). The former are included in the comb-like configurational stripes at $\Theta = 0.5$ ML and $\Theta = 1$ ML; the latter, which have a higher resolution in the Pt concentration x and the coverage Θ, form the smaller stripes.

The $\Theta = 0$ ML case in Fig. 2 reproduces the stability diagram of the clean surface in Ref. 18. The formation energies of the clean surface are minute compared with the energies at $\Theta > 0$ ML, which are dominated by the adsorption energy of C on the alloy's surface. For $\Theta \leqslant 0.5$ ML, this adsorption energy is highest for the hollow adsorption site, and all low-energy structures in that region have carbon adsorbed at hollow sites only. Adsorption at other sites is seen as the higher-energy comb-like form of the configurational scan at $\Theta = 0.5$ ML. When the coverage increases beyond $\Theta = 0.5$ ML, the situation changes. For $\Theta = 1$ ML, the CE predicts structures where many C atoms cluster on adjacent adsorption sites of the adsorbate layer, thus releasing large amounts of energy due to the binding. A whole set of such structures is set energetically apart from the rest by over 20 eV, which is not a plausible result; see Fig. 2(b). However, the fact is that the CE was not converged for such high coverages, and DFT calculations for CE predictions in that region could not provide valid input for the CE at all: the clustering of C atoms generated an extreme buckling of the first substrate layer, which was almost detached from the layers beneath. The pronounced C-C bonds also forced the adsorbate atoms to strongly relax from their ideal adsorption sites; then, they occupied interstitial sites of the adsorbate lattice in such a way that the link between DFT results and the CE lattice is no longer valid, and no longer could the DFT results serve as input for the fixed-lattice CE. Those shortcomings explain why the CE so tremendously overestimates the energy released by the carbon-carbon bonds. Since the coupled CE for $C/Pt_{25}Rh_{75}(100)$ is not converged for $\Theta \geqslant 1$ ML nor can it ever be converged on a lattice that allows adsorbate structures with C-C bonds, the CE energies there are null and void.

The CE Eq. (9) is only converged for the concentration range $0 \leqslant x \leqslant 0.5$ and $0 \leqslant \Theta \leqslant 0.5$. In this region, the configurational predictions in Fig. 2 are correct, and Fig. 3 summarizes the corresponding $T = 0$ K results of the DFT calculations proposed by the cluster expansion: the DFT stability planes (convex hull), the vertices of those planes representing the stable states, and some real-space representations of the structures.

Four characteristics in Fig. 3 are especially noteworthy. First, it is not before $\Theta = 0.33$ ML that the stable states exhibit a tendency to Pt depletion in the first substrate layer. It is there that the segregation energy of Pt is overcome by carbon's preference for Rh. Second, it shows that the stability planes lean towards Pt depletion. This significantly affects all structures that are not vertices of the stability planes, and it affects later MC simulations. The system clearly feels the influence of higher-coverage, lower-Pt-content stable structures. Third, all stable states show C adsorbing at hollow sites, which proves that a restriction to hollow adsorption sites only is valid. Finally, the stable structures at $\Theta = 0.5$ ML answer to the question where the Pt segregates to when the C-Rh bonds dominate. At that high coverage, it is expelled from the first layer into the second layer, after which the fourth layer gets populated when the surface Pt content x is increased, before the third layer (not shown) and, in the end, also the first substrate layer get their share of Pt. At $(x,\Theta) = (0.5,0.5)$, Pt is distributed evenly among the four substrate layers.

It should be mentioned that the presence of carbon not only influences the segregation profile, but also the interlayer relaxations of the alloy surface. The first substrate layer takes up the hollow-site carbon, which in turn exerts a pull on the layer, so that the distance between the first and the second substrate layer is significantly expanded, in accordance with the experimental findings of Ref. 12. This behavior is also observed for lower coverage, albeit less pronounced then.

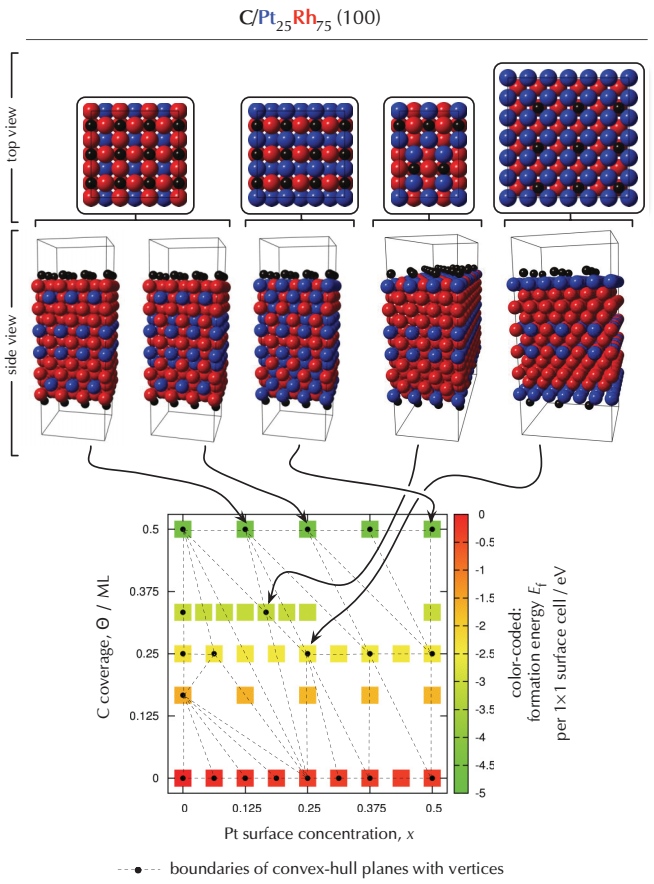

FIG. 3. (Color online) Stability diagram for $C/Pt_{25}Rh_{75}(100)$ based on DFT for the concentration region $0 \leqslant x \leqslant 0.5$ and $0 \leqslant \Theta \leqslant 0.5$. It is a projection of the concentration-energy cube in Fig. 2(a) onto the (x,Θ) plane and constitutes the $T = 0$ K phase diagram. The diagram shows color-coded the DFT formation energy $E_f(\tilde{\sigma},\tilde{\alpha})$ of the energetically lowest structure at each concentration (x,Θ), where DFT calculations had been performed. The dots represent the vertices of the convex-hull hyperplanes, i.e., the stable states of the stability planes for $C/Pt_{25}Rh_{75}(100)$. Almost all stability planes lean towards a higher coverage and a lower Pt content. Note that all stable states even at $\Theta = 0.5$ ML have carbon adsorbed at hollow positions.

B. Adsorbate-induced segregation for higher temperature

The $T = 0$ K results from above are now complemented by canonical MC simulations for $T > 0$ K. Those also cover the configurational entropy, give access to excited configurational states, and thus introduce a temperature scale into the Hamiltonian Eq. (9). Furthermore, a large MC superlattice allows adjustments to the coverage much finer than possible with small DFT cells or comprehensive CE scans.

Unfortunately, Eq. (9) cannot be used for the full lattice L as defined in Sec. II. The problem had already been manifested in Fig. 2. Comparing this figure with Fig. 3, one notices that the DFT stability planes of Fig. 3 will be completely concealed by the CE predictions for $\Theta = 1$ ML. Although we have already dismissed those predictions as unphysical, the Hamiltonian in Eq. (9) does not "know" that those predictions are unphysical. If we ran an MC simulation with Eq. (9) for the full lattice L, the simulation would be aware of the unphysical structures. It is tremendously important to recognize that the "stable states" of the CE at $\Theta = 1$ ML have an impact even on simulations within the concentration ranges $0 \leqslant x \leqslant 0.5$ and $0 \leqslant \Theta \leqslant 0.5$, because those structures obliterate the stable states within the desired concentration range. So, those unphysical structures must be eschewed from the ground up in order to completely avoid them in the Hamiltonian and in the simulation.

During the discussion of Fig. 2, we examined the nature of the unphysical structures at $\Theta = 1$ ML. They hail from clustering C atoms on the fine adsorption lattice, which allows top, bridge, and hollow positions. In order to remove the influence of the unphysical predictions at $\Theta = 1$ ML, we removed the top and bridge sites from the adsorption lattice and retained only the hollow sites. The validity of this approximation rests on the carbon's clear preference for the hollow adsorption sites. All DFT calculations show that for $\Theta \leqslant 0.5$ ML the adsorption energy is highest for this situation, and it is only for higher coverages that the already mentioned C-C bonds in combination with large top-layer relaxations render the topological model of the CE invalid.

The results of canonical MC simulations for $C/Pt_{25}Rh_{75}(100)$ with a Pt surface concentration of $x = 0.25$ are shown in Fig. 4. The choice of $x = 0.25$ is prompted by the results of the clean surface,[18] as well as by experimental data for the system.[12] Both suggest a concentration of roughly 25% Pt within the first four surface layers, for the clean surface as well as the slightly C-contaminated surface. The MC simulations reveal the tremendous impact of even a modest carbon contamination. By the presence of C, the first substrate layer—once the stronghold of Pt segregation for clean surfaces—is more and more depleted of Pt, whereas the layers beneath are more and more enriched with Pt. The small coverages $\Theta \leqslant 12.5\%$ ML are not up to evicting the majority of Pt from the first layer, but a fair amount of Pt has to leave the first layer and occupy the layers beneath.

The impetus for this change in segregation is carbon's preference to bind to Rh instead of Pt. Our simulations exactly exhibited this behavior: The fourfold hollow adsorption sites with a C atom were surrounded by Rh atoms (not shown), which decreased the overall Pt content of the first substrate layer. This binding of C to Rh instead of Pt is so prominent in the simulation that one can even give a rule-of-thumb prediction of the first substrate layer's amount of Pt. Suppose there are N_1 sites in the topmost substrate layer. For the clean surface, approximately all of those N_1 sites are occupied by Pt, at least for low temperatures. There are also N_1 hollow adsorption sites, each of which has four substrate neighbors. Given a coverage Θ, then $N_1\Theta$ of those adsorption sites accommodate a C atom, which in turn force the Pt out of its four substrate neighbors, replacing it with Rh. The binding of C to Rh therefore decreases the Pt content in the topmost layer from 1 to $1 - 4\Theta$. For $\Theta = 12.5\%$ ML this rough estimate yields a Pt content of 50% in the first substrate layer, a little bit lower than the actual simulation. The difference mainly comes from the fact that the occupied adsorbate sites are not totally independent of each other.

The Pt expelled from the first substrate layer especially enriches the fourth layer, far away from the C atoms. The second layer is unfavorable throughout, and it is only the large amount of Pt removed from the first layer that enriches

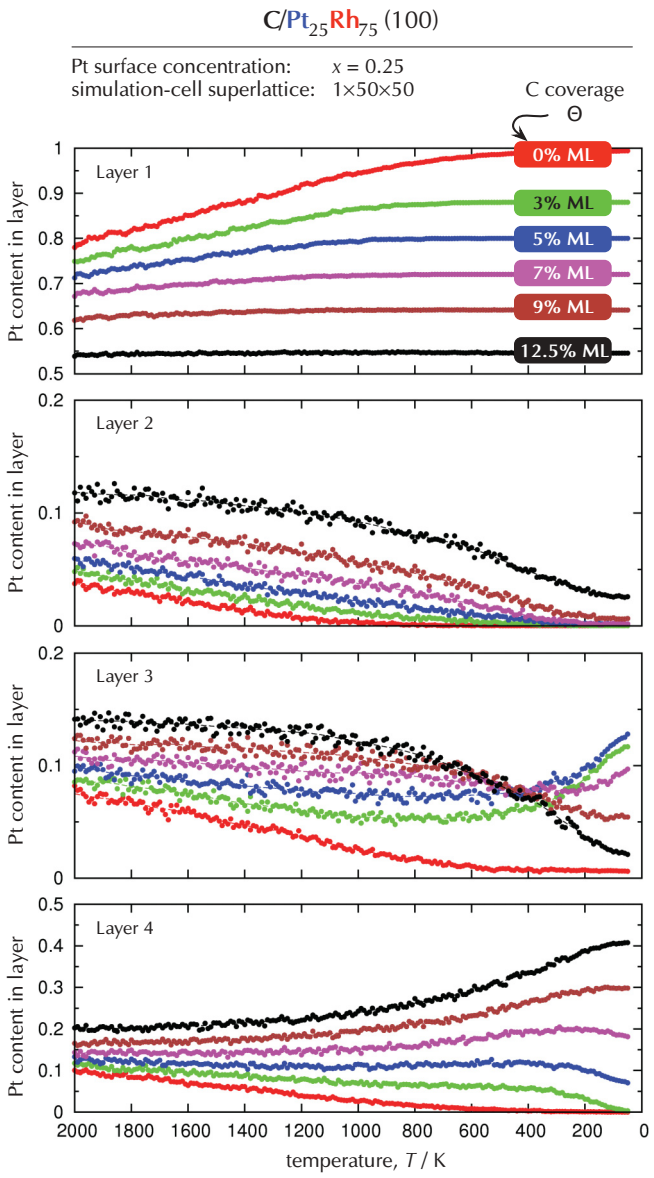

FIG. 4. (Color online) The temperature-dependent segregation profile for $C/Pt_{25}Rh_{75}(100)$ at a fixed Pt surface concentration $x = 0.25$ within the four substrate layers. The data were obtained by simulated annealing with a canonical Monte Carlo simulation. Note the different scales on the ordinate axes. The presence of carbon significantly lowers the Pt content in the first substrate layer and enriches the layers underneath.

the second layer a bit for increasing coverages. Between the third and the fourth layers, there is a fine interplay for temperatures below 500 K. In the case of very small coverages $\Theta \leqslant 5\%$ ML at those temperatures, Pt still succeeds in segregating into the more surface-near third layer, while the equilibrium concentration of Pt in the fourth layer decreases with temperature and bends towards the 0% Pt concentration that is observed for the clean surface at $\Theta = 0\%$ ML (i.e., the fourth layer shows "clean-like behavior"). Higher coverages $\Theta \geqslant 7$ ML change this behavior and deposit more Pt into the fourth layer when the temperature is lowered. The fourth layer is therefore "clean-like" for $\Theta \leqslant 5\%$ ML and "C-adsorbate-like" for $\Theta \geqslant 7$ ML. This alteration can also be observed

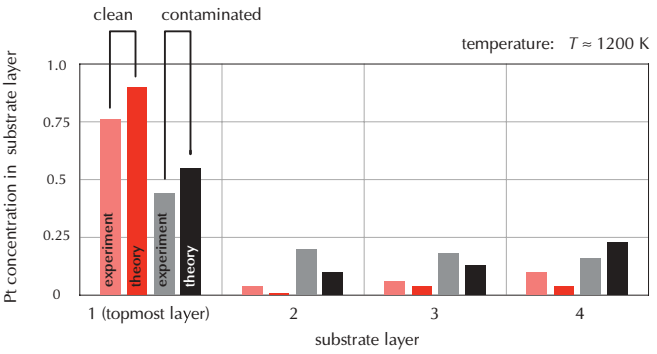

FIG. 5. (Color online) A comparison between the experimental and cluster-expansion segregation profile of $Pt_{25}Rh_{75}(100)$, both for the clean surface and the carbon-contaminated surface. The experimental data result from LEED measurements[12] at $x = 0.24$ with coverages of $\Theta = 0$ ML and $\Theta \approx 0.07$ ML, respectively. The cluster-expansion data stem from the MC simulation shown in Fig. 4. They are for $x = 0.25$ and $\Theta = 0$ ML or $\Theta = 0.125$ ML, respectively.

in the third layer: its crossover in the Pt concentration at $T < 500$ K correlates with the fourth layer's adjustment as a response to the C adsorbates. The impact of C on the third layer—and hence on the fourth layer—is not so much unexpected. Regarding the fact that C at hollow sites relaxes the surface (more strongly for higher coverage) and binds closely to the first-layer atoms (not shown), the third layer is not totally out of reach for the carbon's direct influence.

Figure 5 compares the simulation results with experimental data by Platzgummer *et al.*[12] who performed a quantitative LEED structure analysis to determine the segregation profile. In the experiment, the presence of C on the alloy's surface was not intentional; rather, the Pt-Rh sample was unwittingly contaminated. So, the experimental data do not constitute a systematic study of the adsorption behavior of C and its influence on the segregation profile; neither could the C contamination be quantified with high accuracy. The authors of Ref. 12 determined a level of carbon contamination $\Theta \approx 7\%$ ML. Also the accuracy of the LEED analysis for the segregation profile dwindles with every additional surface layer. With those experimental caveats, the agreement between the data of Platzgummer *et al.*[12] and our simulation results in Fig. 5 for a slightly higher C coverage is rather good.

The coupled CE is thus able to reproduce the experimental segregation profile, albeit with some errors. The errors are to be found on both sides of the comparison: both the LEED experiment and the simulation are not perfect. The problems of the experiment have already been pointed out in the previous paragraph. But what kind of effects does the simulation not take in, and what effects produce deviations from the true segregation profile? There are at least four possible sources of errors in the CE. First, the problems of getting reliable DFT results for $\Theta \geqslant 1$ ML. While those are probably not really necessary from a physical point of view because we are not interested in such high coverages, they influence the construction of a cluster expansion. Related to this point is the second source of error: the approximation of excluding all top and bridge sites from the MC simulation. As has been discussed, this is a regrettable approximation, but an inevitable

one. Third is the restriction of the simulation to canonical MC. It is probably the smallest source of error for the comparison between experiment and theory, as also the experiment finds a Pt surface concentration of $x \approx 0.25$ at $T \approx 1200$ K. Nevertheless, the surface concentration x can in principle change with temperature so that the temperature-dependent segregation profile in Fig. 4 might have to be adapted by small concentration amounts. Last, neither our DFT calculations nor the resulting CE includes phononic contributions, which might well give some decisive difference during the MC simulations; cf. the work of Reith *et al.*[48] While the heavy Pt and Rh atoms might not be influenced by vibrational contributions too much, the vibrations may change the energetics of the lighter C adsorbate and its binding to the substrate.

IV. CONCLUSIONS

In this paper, we advanced the development of a coupled cluster-expansion (CE) approach in the spirit of Refs. 34 and 35, used an averaging of different CE Hamiltonians as in Ref. 48, and thus gained access to the highly complex configuration space for the coupling between a substrate and an adsorbate system, namely, for $C/Pt_{25}Rh_{75}(100)$.

In this configuration space, the influence of carbon adsorbates on the segregation profile of the $Pt_{25}Rh_{75}(100)$ substrate is a power struggle between two competing energies. On the one hand, the substrate system clearly favors the segregation of Pt to the topmost layer; on the other hand, Rh forms the stronger bonds with a C adsorbate. In the end, it comes down to balancing those forces. With the help of the CE, we constructed a stability diagram for a Pt content up to 50% in the four topmost substrate layers and a C coverage below 0.5 monolayers, where all energetically favorable C adsorption was shown to take place at hollow sites. For higher coverage, the simulation had to be actively restricted to those hollow sites, lest the CE Hamiltonian favor nearby C-C bonds characteristic of a coverage above 1 monolayer. So, also the subsequent canonical Monte Carlo (MC) simulations were conducted on a simulation lattice that only allows C adsorption at hollow sites. Our MC results extended the $T = 0$ K stability diagram towards higher temperatures, and we obtained the adsorbate-induced segregation profile for different temperatures and different C coverages. The experimental segregation profile agrees well with our prediction, although we needed to assume a slightly higher C contamination of the substrate.

Although the CE and the MC simulation were subject to some approximations, we demonstrated that a CE can predict the segregation behavior of clean surfaces as well as the changes that adsorbates bring about. With the present developments, adsorbate-induced segregation can now be studied with *ab initio* precision. Furthermore, the couple CE formalism can easily be adapted to other physical systems and general interfaces.

ACKNOWLEDGMENTS

The authors T.C.K. and S.M. gratefully acknowledge the support of the German Research Foundation (DFG) under Project No. MU1648/2. R.P. gratefully acknowledges support of the the Austrian Science Fund (FWF) within the Special Research Program "ViCoM". Calculations were performed partly on the high-performance clusters of the University of Erlangen, the Hamburg University of Technology, and on the Vienna Scientific Cluster (VSC).

*tobias.kerscher@tuhh.de

[1] C. W. Davis, US Patent No. 1,706,055 (1929).
[2] C. W. Davis, US Patent No. 1,850,316 (1932).
[3] C. D. Keith and C. E. Cunningham, US Patent No. 3,441,381 (1969).
[4] Z. Hu, F. M. Allen, C. Z. Wan, R. M. Heck, J. J. Steger, R. E. Lakis, and C. E. Lyman, J. Catal. **174**, 13 (1998).
[5] B. R. Powell and Y.-L. Chen, App, Catalysis **53**, 233 (1989).
[6] M. Shelef and R. W. McCabe, Catal. Today **62**, 35 (2000).
[7] H. S. Gandhi, G. W. Graham, and R. W. McCabe, J. Catal. **216**, 433 (2003).
[8] J. Hangas and A. E. Chen, Catal. Lett. **108**, 103 (2006).
[9] R. E. Lakis, C. E. Lyman, and H. G. Stegner, J. Catal. **154**, 261 (1995).
[10] R. E. Lakis, Y. Cai, H. G. Stegner, and C. E. Lyman, J. Catal. **154**, 276 (1995).
[11] P. Granger, J. J. Lecomte, L. Leclercq, and G. Leclercq, Appl. Catal., A **208**, 369 (2001).
[12] E. Platzgummer, M. Sporn, R. Koller, S. Forsthuber, M. Schmid, W. Hofer, and P. Varga, Surf. Sci. **419**, 236 (1999).
[13] C. Steiner, B. Schönfeld, M. M. I. P. van der Klis, G. Kostorz, B. D. Patterson, and P. R. Willmott, Phys. Rev. B **73**, 174205 (2006).
[14] Z. W. Lu, S.-H. Wei, and A. Zunger, Phys. Rev. Lett. **66**, 1753 (1991).
[15] L. Z. Mezey and W. Hofer, Surf. Sci. **402**, 845 (1998).
[16] K. Yuge, A. Seko, A. Kuwabara, F. Oba, and I. Tanaka, Phys. Rev. B **74**, 174202 (2006).
[17] S. Müller, M. Stöhr, and O. Wieckhorst, Appl. Phys. A **82**, 415 (2006).
[18] P. Welker, O. Wieckhorst, T. C. Kerscher, and S. Müller, J. Phys.: Condens. Matter **22**, 384203 (2010).
[19] F. L. Williams and G. C. Nelson, Appl. Surf. Sci. **3**, 409 (1979).
[20] F. C. M. J. M. van Delft, A. D. van Langeveld, and B. E. Nieuwenhuys, Surf. Sci. **189-190**, 1129 (1987).
[21] J. Siera, F. C. M. J. M. van Delft, A. D. van Langeveld, and B. E. Nieuwenhuys, Surf. Sci. **264**, 435 (1992).
[22] P. T. Wouda, B. E. Nieuwenhuys, M. Schmid, and P. Varga, Surf. Sci. **359**, 17 (1996).
[23] E. L. D. Hebenstreit, W. Hebenstreit, M. Schmid, and P. Varga, Surf. Sci. **441**, 441 (1999).
[24] D. P. Woodruff, M. A. Muñoz-Márquez, and R. E. Tanner, Current App. Phys. **3**, 19 (2003).
[25] V. Drchal, A. Pasturel, R. Monnier, J. Kudrnovsky, and P. Weinberger, Comput. Mater. Sci. **15**, 144 (1999).
[26] S. Müller, Surf. Interface Anal. **38**, 1158 (2006).
[27] J. Luyten, M. Schurmans, C. Creemers, B. S. Bunnik, and G. J. Kramer, Surf. Sci. **601**, 1668 (2007).

[28]K. Yuge, Phys. Rev. B **84**, 085451 (2011).
[29]A. Baraldi, D. Giacomello, L. Rumiz, M. Moretuzzo, S. Lizzit, F. B. de Mongeot, G. Paolucci, G. Comelli, R. Rosei, B. Nieuwenhuys, U. Valbusa, and M. Kiskinova, J. Am. Chem. Soc. **127**, 5671 (2005).
[30]M. Sporn, E. Platzgummer, E. Gruber, M. Schmid, W. Hofer, and P. Varga, Surf. Sci. **416**, 384 (1998).
[31]J. M. Sanchez, F. Ducastelle, and D. Gratias, Physica A **128**, 334 (1984).
[32]J. W. D. Connolly and A. R. Williams, Phys. Rev. B **27**, 5169 (1983).
[33]G. D. Garbulsky and G. Ceder, Phys. Rev. B **51**, 67 (1995).
[34]P. D. Tepesch, G. D. Garbulsky, and G. Ceder, Phys. Rev. Lett. **74**, 2272 (1995).
[35]B. C. Han, A. Van der Ven, G. Ceder, and B.-J. Hwang, Phys. Rev. B **72**, 205409 (2005).
[36]D. Lerch, O. Wieckhorst, G. L. W. Hart, R. W. Forcade, and S. Müller, Modell. Simul. Mater. Sci. Eng. **17**, 055003 (2009).
[37]E. Raub, J. Less-Common Met. **1**, 3 (1959).
[38]*Binary Alloy Phase Diagrams*, edited by T. B. Massalski (ASM International, Materials Park, OH, 1990), Chap. Pt-Rh (Platinum-Rhodium).
[39]C. Steiner, B. Schönfeld, M. J. Portmann, M. Kompatscher, G. Kostorz, A. Mazuelas, T. Metzger, J. Kohlbrecher, and B. Demé, Phys. Rev. B **71**, 104204 (2005).
[40]J. Pohl and K. Albe, Acta Mater. **57**, 4140 (2009).
[41]S. B. Maisel, T. C. Kerscher, and S. Müller, Acta Mater. **60**, 1093 (2012).
[42]C. Wolverton and D. de Fontaine, Phys. Rev. B **49**, 8627 (1994).
[43]G. L. W. Hart, V. Blum, M. J. Walorski, and A. Zunger, Nat. Mater. **4**, 391 (2005).
[44]L. G. Ferreira, S.-H. Wei, and A. Zunger, Inter. J. Supercomp. Appl. **5**, 34 (1991).
[45]S. Müller, J. Phys.: Condens. Matter **15**, R1429 (2003).
[46]F. Lechermann, M. Fähnle, and J. M. Sanchez, Intermetallics **13**, 1096 (2005).
[47]R. Drautz, H. Reichert, M. Fähnle, H. Dosch, and J. M. Sanchez, Phys. Rev. Lett. **87**, 236102 (2001).
[48]D. Reith, M. Stöhr, R. Podloucky, T. C. Kerscher, and S. Müller, Phys. Rev. B **86**, 020201(R) (2012).
[49]G. Kresse and J. Hafner, Phys. Rev. B **47**, 558 (1993).
[50]G. Kresse and J. Hafner, J. Phys.: Condens. Matter **6**, 8245 (1994).
[51]G. Kresse and J. Furthmüller, Phys. Rev. B **54**, 11169 (1996).
[52]G. Kresse and J. Furthmüller, Comput. Mater. Sci. **6**, 15 (1996).
[53]G. Kresse and D. Joubert, Phys. Rev. B **59**, 1758 (1999).
[54]P. E. Blöchl, Phys. Rev. B **50**, 17953 (1994).
[55]J. P. Perdew, J. A. Chevary, S. H. Vosko, K. A. Jackson, M. R. Pederson, D. J. Singh, and C. Fiolhais, Phys. Rev. B **46**, 6671 (1992).
[56]H. J. Monkhorst and J. D. Pack, Phys. Rev. B **13**, 5188 (1976).